Density Functional Theory Study of Water Activation and CO_{ads} + OH_{ads} Reaction on Pure Platinum and Bimetallic Platinum/Ruthenium Nanoclusters

Alejandro Perez, Marius J. Vilkas, Carlos R. Cabrera, and Yasuyuki Ishikawa*

Department of Chemistry and the Chemical Physics Program, University of Puerto Rico, P.O. Box 23346, San Juan, PR 00931-3346

A density functional theory study of the elementary steps that lead to the removal of $CO_{ads(Pt)}$ over alloyed and sequentially deposited Pt/Ru bimetallic nanoclusters is presented. The reaction energies and activation barriers for the $H_2O_{ads(Ru)}$ dissociation and $CO_{ads(Pt)}$ + $OH_{ads(Ru)}$ reaction are estimated in solid−gas interface and in a microsolvated environment to determine which surface morphology is more tolerant to CO_{ads} poisoning. On the basis of the energetics, the sequentially deposited Pt/Ru nanocluster is predicted to be a much more promising anode catalyst than the alloy cluster surface in fuel cell applications.

1. Introduction

The direct methanol fuel cell (DMFC) is an attractive power source for mobile applications due to the high energy density of methanol, the portability and ease of distribution of liquid rather than gaseous fuel, and elimination of the need for a bulky, power-consuming fuel re-former. Because of its portability and ease of distribution of fuel, DMFC is among the most promising compact power sources for communication devices. However, several factors limits the power output of polymer electrolyte DMFCs. The slow kinetics of the methanol electrooxidation reaction on conventional anode catalyst materials is one of the major factors.
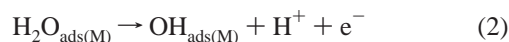
To improve the efficiency of fuel cells and reduce production costs, nanoparticles of noble metals are commonly employed in the design of catalysts due to their higher catalytic activity over bulk metal surfaces. Platinum has been used as a primary electrode material because of its relatively high catalytic activity and stability. Although this metal is well suited for the dehydrogenation of hydrocarbons and alcohols on anode of an electrochemical cell, it is easily poisoned by carbon monoxide: concentrations as little as 20 ppm significantly degrade the performance of pure Pt catalyst,[1] and this continues to be one of the major obstacles in the development of efficient low-temperature fuel cells. This surface poison is the product or the intermediate in the partial oxidation of organic molecules at the anode of the electrochemical cell, and it is typically found in trace amounts in the hydrogen gas from the steam-reformed hydrocarbons. The presence of oxygenated species, such as OH and O, from the activation of ambient water on the catalyst is believed to mitigate, but not eliminate, the blocking effect of CO at moderate potentials. The overall reaction is commonly written as follows:

$$H_2O_{ads} + CO_{ads} \rightarrow CO_2 + 2H^+ + 2e^- \qquad (1)$$
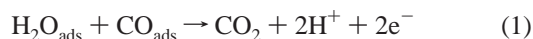
On pure Pt anode, the rate of oxidative stripping of CO_{ads} from Pt sites at moderate potential is not sufficiently high and the activation of $H_2O_{ads(Pt)}$ is very difficult, leading to a rapid

decrease in the rate of dehydrogenation reactions and, consequently, in the current.

Intense research has been carried out to minimize the vulnerability of Pt-based anode materials to CO poisoning. Today, most of efforts to overcome the blocking effect of CO_{ads} on Pt anode have focused on alloying Pt with a secondary metal M. The enhancement effect of M is attributed to a *bifunctional mechanism* posited by Watanabe and Motoo.[2,3] Pt serves to adsorb and dehydrogenate methanol or other organic fuel, while M provides the nucleation sites for the formation of active oxidant $OH_{ads(M)}$—reaction 2. Once the surface hydroxyl intermediate $OH_{ads(M)}$ is formed at M sites, it oxidizes the $CO_{ads(Pt)}$ on neighboring Pt sites to CO_2—reaction 3—facilitating removal of the poisoning agents. The $COOH_{ads(Pt)}$ intermediate has been detected by Watanabe et al. using infrared spectroscopy techniques.[4,5]

$$H_2O_{ads(M)} \rightarrow OH_{ads(M)} + H^+ + e^- \qquad (2)$$

$$CO_{ads(Pt)} + OH_{ads(M)} \rightarrow COOH_{ads(Pt)} \rightarrow CO_2 + H^+ + e^- \quad (3)$$

Alloyed Pt/Ru nanoparticles have attracted considerable attention as promising catalysts.[6−9] Currently, most of the anodic materials in DMFC are manufactured using Pt/Ru alloys. Investigations of the alloy electrodes have established that a Pt/Ru alloy of 50:50 composition has the highest catalytic activity for CO electrooxidation.

In the quest for better anode materials, several Pt/Ru systems have been investigated from various standpoints, such as those of morphology, composition, and dispersion state to establish how these factors affect the electrooxidation current. Recently, bimetallic nanoclusters obtained by depositing Ru atoms on Pt principal nanoparticles have attracted considerable interest. Wieckowski et al.[10] have reported that Ru islands deposited on Pt nanoparticles are more electrocatalytically active than are surfaces in which Ru is alloyed with Pt. Subsequent experimental studies by Lin et al.[11] and Davies et al.[12] have also confirmed these experimental findings, and the latter has proposed two different routes for the oxidative removal of CO on these surfaces. More recently, Cabrera et al.,[13] using a similar strategy, have demonstrated the high catalytic activity of these surfaces, especially at low Ru coverage for methanol oxidation.

* Corresponding author. E-mail: ishikawa@rrpac.upr.clu.edu. Fax: (787) 756-7717.

We present a comparative theoretical study of alloyed Pt/Ru and sequentially deposited Pt/Ru nanoclusters at the potential of zero total charge. The aim is to identify which morphology featured in the Pt/Ru systems enhances the dissociation of water and CO_{ads} oxidation, leading to more CO-tolerant anode materials for low-temperature fuel cells. Through a set of density functional theory (DFT)[14,15] calculations, we examine the energetics of H_2O_{ads} dissociation and $CO_{ads} + OH_{ads}$ reaction on bimetallic nanoparticles of varying morphology. The effects on the activation barriers of alloying Ru with Pt or sequentially depositing Ru on Pt are studied in model nanoscale clusters. Under the assumption of the *bifunctional mechanism*, we address the problem of CO poisoning on pure Pt nanoparticles, and provide insight into the mechanism that governs the CO_{ads} removal from the Pt sites of different bimetallic nanoclusters. The goal of this study is to understand at the atomic level the origin of the apparent higher catalytic activity of the bimetallic nanocluster surfaces formed by sequential deposition of Ru on Pt over the alloyed surfaces.

2. Methods

All calculations were performed using the DFT code DMol[3] of Accelrys Inc.[16,17] The Kohn−Sham orbitals were expanded in a numerical basis set of double + polarization quality (dnp). The Perdew−Burke−Ernzerhof[18] (PBE) exchange and correlation functionals were employed. The all-electron scalar relativistic correction[19] for use with density functionals in DMol[3] was employed to obtain more accurate energetics and to reproduce the right site preferences. For geometry optimizations, the interaction of valence electrons with the cores was described by semicore pseudopotentials DSPP.[16,17]

The reaction paths were mapped to locate the transition states (TS). The distance between the relevant species was changed in a pointwise fashion, and the partial optimization was continued with a minimization of the total energy with respect to all remaining degrees of freedom. Only those metal atoms of the top layer directly involved in the reaction were permitted to relax in the calculations. The underlayer was completely frozen in all optimizations. The configuration that exhibits the maximum energy along the reaction path was subjected to a partial frequency analysis to confirm the presence of a single imaginary frequency, indicative of a first-order saddle point in the potential energy surface.

In our calculations, the fractional occupation number technique[20] was adopted to account for the large number of unoccupied orbitals lying close to the Fermi level in a large metal cluster. The electrons are "smeared" within 0.1 eV kcal/mol above the HOMO following approximately a Fermi distribution at finite temperature.

3. Metal Surface Modeling

Both pure Pt and bimetallic Pt/Ru surfaces exhibit a fcc crystal structure. The low-index face (111) was taken as the representative surface for the present study because it is known to exhibit one of the highest electrocatalytic activities. Parts a−c of Figure 1, respectively, display the geometrical structures of the pure Pt, alloy, and sequentially deposited bimetallic clusters. For the pure platinum cluster, the structure employed in an earlier study[21] was adopted. The model comprises two layers with 19 atoms each. The bulk Pt−Pt bond distance from experimental data (cell parameter $a = 3.92$ Å) was initially adopted in all clusters. Relaxation was permitted only for those metal atoms of the surface layer more directly involved in the reaction.

Earlier experimental studies[22] have shown that the effect of alloyed Ru on the electrooxidation is evident only if Ru is present in the top surface layer. Thus, to simulate the (111) surface of the Pt/Ru alloy nanoparticle, a surface Pt atom of the Pt_{38} cluster was substituted by a Ru atom to create a surface alloy. Only the surface layer Pt atoms and Ru were allowed to vary their positions in the optimizations. The surface Ru atom assumes the optimum position slightly below the top Pt layer (~0.25 Å).

Recent experimental studies have shown that the sequential deposition of ruthenium on Pt(111) leads to Ru layers, mostly monatomic at low coverages.[12,23] Furthermore, Cabrera et al.[13] have shown that the relatively low surface Ru coverage produces the highest electrocatalytic activities of bimetallic nanoclusters. Therefore, to simulate the sequential deposition of Ru on Pt-(111), a single Ru atom was placed above the surface layer of the Pt_{38} nanocluster, leading to $Pt_{38}Ru$. Only the Ru and surrounding Pt positions in the top layer were optimized. The optimum position of the ruthenium atom was at a 3-fold hollow site above the top layer.

4. Results and Discussion

4.1. Adsorption of CO on Pt and Bimetallic Pt/Ru Nanoparticles. The adsorption of CO on Pt(111) has been extensively studied both theoretically and experimentally. The adsorption energies (E_{ads}) and the site preference of $CO_{ads(Pt)}$ over different clusters were examined. The adsorption energy for an adsorbate is defined as follows:

$$E_{ads} = E_{adsorbate} + E_{cluster} - E_{(cluster-adsorbate)}$$

where $E_{(cluster-adsorbate)}$, $E_{cluster}$, and $E_{adsorbate}$ are, respectively, the total energies of the complex (metal cluster and adsorbate), metal cluster alone, and the free adsorbate.

An all-electron scalar relativistic calculation was shown to be essential to predict the right adsorption sites (top) and binding energies. The all-electron calculations predict that the top site is nearly 4 kcal/mol more stable than the bridge and 1 kcal/mol more stable than 3-fold hollow site. This is in contrast with numerous slab DFT studies in which the position of the CO is erroneously predicted to prefer the 3-fold (fcc) site. This artifact of the DFT calculations has been widely discussed in the literature.[24−26] The calculated binding energy for CO on pure Pt_{38}(111), 37.0 kcal/mol, is in good agreement with recent slab calculations by Koper et al.[27] on CO atop the Pt site ($E_{ads} = 37.6$ kcal/mol).

The introduction of the secondary metal Ru has a small effect on the adsorption of CO to Pt sites. The weakening effect in the Pt−CO bond, the so-called *ligand effect*,[28] is slightly greater on the alloy ($E_{ads} = 35.4$ kcal/mol) than on the sequentially deposited Pt/Ru ($E_{ads} = 36.4$ kcal/mol). The differences in adsorption energies with respect to pure Pt are so small that the *ligand effect* is of little importance here, and the promoting effect of Ru must be ascribed entirely to a bifunctional mechanism.

4.2. Dissociation of H_2O_{ads} on Pure Pt and on the Ru Sites in Pt/Ru Nanoclusters. To understand the catalytic role of water in the oxidative removal of CO_{ads}, we have investigated the energetic cost of generating the oxidant hydroxyl intermediate (OH_{ads}) from the dissociation of H_2O_{ads} over the pure Pt and bimetallic surfaces. In the next subsections, the reaction energies and activation barriers for the dissociation of H_2O_{ads} on pure Pt and on the Ru sites in alloyed and sequentially deposited Pt/Ru nanoclusters are presented. Calculations were carried out in the

Pure Pt and Bimetallic Pt/Ru Nanoclusters

J. Phys. Chem. B, Vol. 109, No. 49, 2005 **23573**

TABLE 1: Activation Barriers for H_2O_{ads} Activation and $CO_{ads} + OH_{ads}$ Reaction over Various Clusters at the Solid−Gas Interface and in a Microsolvated Environment[a]

clusters (111)	H_2O_{ads} dissociation		$CO_{ads} + OH_{ads}$ reaction	
	solid−gas	microsolvation	solid−gas	microsolvation
Pt_{38}	22.8 (18.3)	6.4 (6.4)	5.3 (−10.1)	4.9 (−10.8)
$Pt_{37}Ru_{alloy}$	19.9 (13.7)	4.5 (4.3)	6.4 (−1.9)	6.1 (−10.6)
$Pt_{38}Ru_{sd}$	9.3 (0.0)	0.9 (0.3)	15.2 (+11.3)	3.9 (−6.9)

[a] The reaction enthalpies are given in parentheses. All energies are in kcal/mol.

TABLE 2: Calculated Activation Energies (kcal/mol) for Water Dissociation and CO_{ads} Oxidation on Pt_{38} Cluster, Bulk Pt(111), and Bimetallic Pt/Ru Surfaces[a]

(111) face	H_2O_{ads} dissociation		$CO_{ads} + OH_{ads}$ reaction	
	solid−gas	liquid phase	solid−gas	liquid phase
Pt_{38} cluster[b]	22.8 (+18.3)		5.3 (−10.1)	
Pt slab[c]	34.0 (+12.7)		20.6 (+5.0)	
Pt slab[d]	15.7 (+10.8)		10.2 (+0.5)	
Pt slab[e]			13.4 (−13.8)	
$Pt_{37}Ru$ cluster[b]	19.9 (+13.7)	4.5 (+4.3)	6.4 (−1.9)	6.1 (−10.6)
$Pt_{66.7\%}Ru_{33.3\%}$ slab[c]	25.1 (+12.7)	6.5 (+6.2)	17.0 (+2.6)	14.3 (−1.4)

[a] The values in parentheses are calculated reaction enthalpies. [b] This work. Microsolvated environment. [c] Reference 47. [d] References 48 and 49. [e] Reference 27.

absence of an aqueous medium (conditions prevalent in a reformer) and in the presence of some degree of solvation. The preliminary results of the following subsections have recently been reported elsewhere by the authors.[29] Activation barriers and reaction energies for the water dissociation on the various clusters are listed in Table 1.

4.2.1. Solid−Gas Interface. In solid−gas interface, the Pt_{38} cluster binds H_2O weakly. The calculated E_{ads} of 8.7 kcal/mol is in reasonable agreement with the experimental adsorption energy 9.7 kcal/mol for bulk Pt(111).[30] The water molecule preferentially binds to the Pt atom by its oxygen atom with the molecular plane lying nearly parallel to the surface, similar to what Michaelides et al.[31] found on bulk Pt(111). The $H_2O_{ads(Pt)}$ monomer dissociates over the Pt cluster homolytically, leading to the formation of a metal hydride and a hydroxyl intermediate (OH_{ads}). The TS for the $H_2O_{ads(Pt)}$ dissociation on pure Pt in vapor phase is located at the O−H stretch of 1.61 Å. The activation energy is as high as 22.8 kcal/mol, and the surface dissociation endothermic by 18.3 kcal/mol. In a previous study,[32] the activation and reaction energies were calculated for the same process but on a Pt_9 cluster using the UBI-QEP approach of Shustorovich and Sellers.[33] The estimated activation barrier, 23.5 kcal/mol, and reaction endothermicity, 18.7 kcal/mol, are in good agreement with the findings of the present study.

In Table 2, the activation energies for water dissociation on bulk Pt(111) and Pt/Ru alloy surfaces from two independent DFT slab calculations are compared with those on the pure Pt_{38} and alloy $Pt_{37}Ru$ clusters. $H_{ads(Pt)}$ and $OH_{ads(Pt)}$ are more strongly adsorbed on bulk Pt(111) than on Pt_{38} cluster. The calculated adsorption energies for $H_{ads(Pt)}$ on the Pt_{38} cluster and on bulk Pt(111) are, respectively, 62 and 67 kcal/mol.[49] The calculated adsorption energy for $OH_{ads(Pt)}$ on Pt_{38} is 42 kcal/mol[29] whereas it is much higher at 52−53 kcal/mol[27,31] at a top site of bulk Pt(111). Therefore, the surface-mediated water dissociation on bulk Pt(111), which forms more strongly bound $OH_{ads(Pt)}$ and $H_{ads(Pt)}$, is more facile than that on the Pt_{38} cluster. At the solid−gas interface, the activation barrier, 15.7 kcal/mol, and reaction endothermicity, +10.8 kcal/mol, for water dissociation on bulk

Pt(111) reported by Hu et al.[48] are indeed noticeably lower than those on Pt_{38} cluster. This is in marked contrast to the activation barrier (34 kcal/mol) predicted by Desai and Neurock, which is significantly higher than that on the Pt_{38} cluster.

The cleavage of the O−H bond in $H_2O_{ads(Pt)}$ on pure Pt is very difficult in the vapor phase; at moderate temperature, the water would probably desorb rather than dissociate. Ab initio molecular dynamics simulations have shown the inert nature of the water bilayer on pure Pt(111).[34] Experimental studies have confirmed the stability of water bilayer on pure Pt(111).[35] The structure of the nascent $OH_{ads(Pt)}$ shows a configuration resembling an sp^3 hybridization with the oxygen atom atop the Pt atom, in agreement with a recent UHV study.[36] The hydrogen atom is strongly bound atop Pt. The calculated adsorption energy, 62.0 kcal/mol, agrees well with the experimental value, 60.9 kcal/mol, for H_{ads} on bulk Pt(111).[37]

On the bimetallic Pt/Ru nanoclusters, H_2O_{ads} is preferentially adsorbed atop Ru. On the alloy surface, the water molecular plane remains nearly parallel to the top layer, as in pure Pt, with a binding energy of 15.8 kcal/mol. On the sequentially deposited Pt/Ru nanocluster, the water molecule is also adsorbed on Ru site by the oxygen atom, but it is tilted with the hydrogen atoms pointing directly to the Pt surface (Figure 2b) with a greater adsorption energy (21.2 kcal/mol), reflecting the oxophilic nature of Ru.

Parts a and b of Figure 2, respectively, display the energy profile of water dissociation on the alloy and sequentially deposited Pt/Ru nanoclusters at solid−gas interface. As in pure Pt, H_2O_{ads} dissociates homolytically, leading to radical $OH_{ads(Ru)}$ and surface hydride $H_{ads(Pt)}$ atop the corresponding metal atoms. On alloy, the activation energy for the homolytic water dissociation atop the alloyed Ru is still quite high, at 20.0 kcal/mol, only 3 kcal less than on pure Pt. The 19.4 kcal/mol activation barrier, evaluated earlier[32] by the UBI-QEP approach[33] on a Pt_9Ru alloy, is in good agreement with the present study. The TS is located at the O−H distance in $H_2O_{ads(Ru)}$ of 1.61 Å, like in pure Pt cluster. The process is again endothermic by 13.7 kcal/mol.
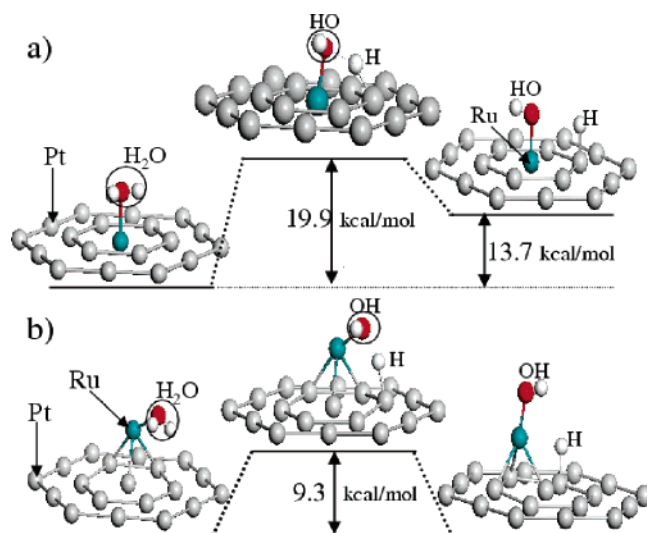
On the sequentially deposited Pt/Ru cluster, the TS for the $H_2O_{ads(Ru)}$ dissociation is located at the O−H separation of 1.57 Å. The calculated activation energy is only 9.3 kcal/mol, and the surface dissociation nearly isothermal with respect to the reactants—a dramatic reduction of the activation barrier and reaction endothermicity. The large reduction in both the activation barrier and the endothermicity can be ascribed to the higher affinity of the Ru adatom toward OH adsorption. Ruthenium's ability toward water activation is also evident in the partially dissociated nature of the water bilayer on bulk Ru-(0001) predicted computationally by Feibelman[38] and by Michaelides et al.[39] Very recently, Held and co-workers[40] have confirmed this conjecture using high-resolution X-ray photoelectron spectroscopy (HRXPS). Therefore, the sequentially deposited Pt/Ru nanocluster entails two advantages over the alloy. First, the presence of undercoordinated Ru atoms highly dispersed over the Pt surface enhances the production of oxidant OH_{ads}; second, the relative abundance of surface Pt atoms facilitates the oxidative reactions. These results clearly suggest that bimetallic Pt/Ru nanoclusters formed by sequential deposition have much higher activity than do alloy clusters in dissociating water and forming oxidant OH_{ads}.

4.2.2. Microsolvated Environment. To simulate the aqueous media around the H_2O_{ads} atop Ru, up to six water molecules were introduced to create a microsolvated environment in the spirit of Anderson and co-workers[41a] who modeled the elec-
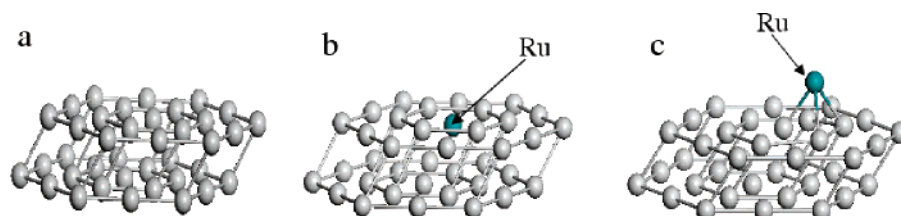
Figure 1. Cluster model structures used in the calculations: (a) Pt_{38} cluster, (b) alloy $Pt_{37}Ru$ cluster, and (c) sequentially deposited Ru on Pt_{38} cluster.

Figure 2. Optimized geometries and energy profile for the $H_2O_{ads(Ru)}$ dissociation at the solid−gas interface on a) alloy $Pt_{37}Ru$ cluster and (b) sequentially deposited Ru on Pt_{38} cluster. The second layer is not shown for clarity.

trooxidation of water on a Pt dimer. Anderson et al. pioneered the application of quantum-mechanical methods (atom superposition and electron delocalization molecular orbital: ASED-MO) to model the H_2O dissociation and CO oxidation on Pt and Pt/Ru clusters.[41b,c] Wang and Balbuena also successfully simulated the electroreduction of O_2 on the Pt(111) surface using the microsolvation model.[42] The ambient water molecules were allowed to move freely during the optimizations. There is a sufficient number of them to allow the proton to fluctuate between a variety of structures such as $H_5O_2^+$ and $H_9O_4^+$, the main intermediates that stabilize the proton in aqueous media.[43−45] The microsolvated environment clearly favors a heterolytic cleavage of the O−H bond in $H_2O_{ads(Ru)}$ where the separation of charges in the TS and products is effectively stabilized by the ambient water molecules. The dissociation reaction generates an $OH_{ads(Ru)}$ and a hydrated proton, with the electron delocalized between the $OH_{ads(Ru)}$ and the entire Pt cluster (eq 2).

A total of five water molecules surrounding the $H_2O_{ads(Ru)}$ were necessary to obtain converged activation barriers for water dissociation on alloy. The presence of the ambient water molecules has a significant effect on the energetics in alloy. It lowers the activation barrier to 4.5 kcal/mol, a significant decrease from a high of 20.0 kcal/mol in the gas phase. The reaction endothermicity also decreases significantly, from 13.7 kcal/mol in the gas phase, to 4.3 kcal/mol in the aqueous media. Figure 3a shows the geometrical arrangement of the microsolvation environment on alloy cluster. In the reactant complex, four of the five water molecules create a five membered ring with the $H_2O_{ads(Ru)}$ and also interact with the Pt surface through their hydrogen atoms. The $H_2O_{ads(Ru)}$ is hydrogen-bonded to the fifth water molecule through its remaining H atom. The O1−H1, H1−O2, O2−H2, and H2−O3 distances in the reactant

complex are, respectively, 1.03, 1.49, 1.00, and 1.62 Å. The TS is located at the O1−H1 distance of 1.49 Å. The H_3O^+ species is clearly formed at the O3 center, and it is separated from the nascent $OH_{ads(Ru)}$ by an intervening water molecule. The H1−O2, O2−H2, and H2−O3 distances at this stage are, respectively, 1.02, 1.35, and 1.09 Å. The configuration of the products resembles the transition state, with the H_3O^+ species remaining at the same position. The Ru−O1 distance shortens to 2.03 Å in comparison to its value in the reactant complex, 2.17 Å, indicating the formation of an incipient OH_{ads} hydroxyl intermediate. The O1−H1, H1−O2, O2−H2, and H2−O3 distances in the dissociation product are, respectively, 1.57, 1.01, 1.41, and 1.06 Å.

For the sequentially deposited Pt/Ru nanocluster, the barrier for the heterolytic dissociation of water atop the Ru adatom is very low, 0.9 kcal/mol. A total of six water molecules were necessary to achieve quantitative convergence in the activation energy. Figure 3b shows the geometrical arrangement of the ambient water molecules around the Ru adatom. In the reactant complex, four of the six water molecules create a hydrogen-bonded five-membered ring, involving the adsorbed $H_2O_{ads(Ru)}$, as in alloy. The other two remain opposite the five membered ring. One of these is attached to the Ru adatom, and the other interacting through hydrogen bonding with the two waters adsorbed on the Ru. The O1−H1, H1−O2, O2−H2, and H2−O3 distances in the reactant complex are, respectively, 1.06, 1.40, 1.00, and 1.58 Å. The transition state was located at the O1−H1 separation of 1.40 Å. Figure 3b clearly shows the formation of a solvated H_3O^+ species at the O2 center, adjacent to the nascent $OH_{ads(Ru)}$ at this stage. The H1−O2, O2−H2, and H2−O3 distances in the transition state are 1.06, 1.11, and 1.31 Å, respectively. Upon dissociation, one of the protons, H2, of the nascent H_3O^+ migrates to the adjacent water, leading to a stable hydronium species flanked by two water molecules. The O1−H1, H1−O2, O2−H2, and H2−O3 distances in the dissociated state are 1.64, 0.99, 1.40, and 1.06 Å, respectively. The Ru−O1 distance shortens from 2.12 Å in the reactant complex to 2.0 Å after the dissociation. The product is nearly isoenergetic to the initial reactant complex, with a negligible difference in energy (0.3 kcal).

In Figure 4, the Mulliken charges on Pt cluster, OH_{ads}, and $H^+(H_2O)_3$ are mapped as a function of the dissociating O−H distance in $H_2O_{ads(Ru)}$. The figure reveals that there already exists a significant separation of charges at the reactant complexes in aqueous media in favor of the subsequent heterolytic O−H bond cleavage. The separation of charges is more pronounced in the sequentially deposited Pt/Ru than it is in alloy. As the dissociating O−H bond elongates, there is a progressive accumulation of negative charge in the Pt cluster and in the OH_{ads}, as well as of positive charge in the ambient water molecules. A plateau in the charge plot is observed at ∼1.49 Å in alloy and at ∼1.40 Å in sequentially deposited Pt/Ru, indicating that the charge transfer is nearly complete at these internuclear distances.

Pure Pt and Bimetallic Pt/Ru Nanoclusters

J. Phys. Chem. B, Vol. 109, No. 49, 2005 **23575**
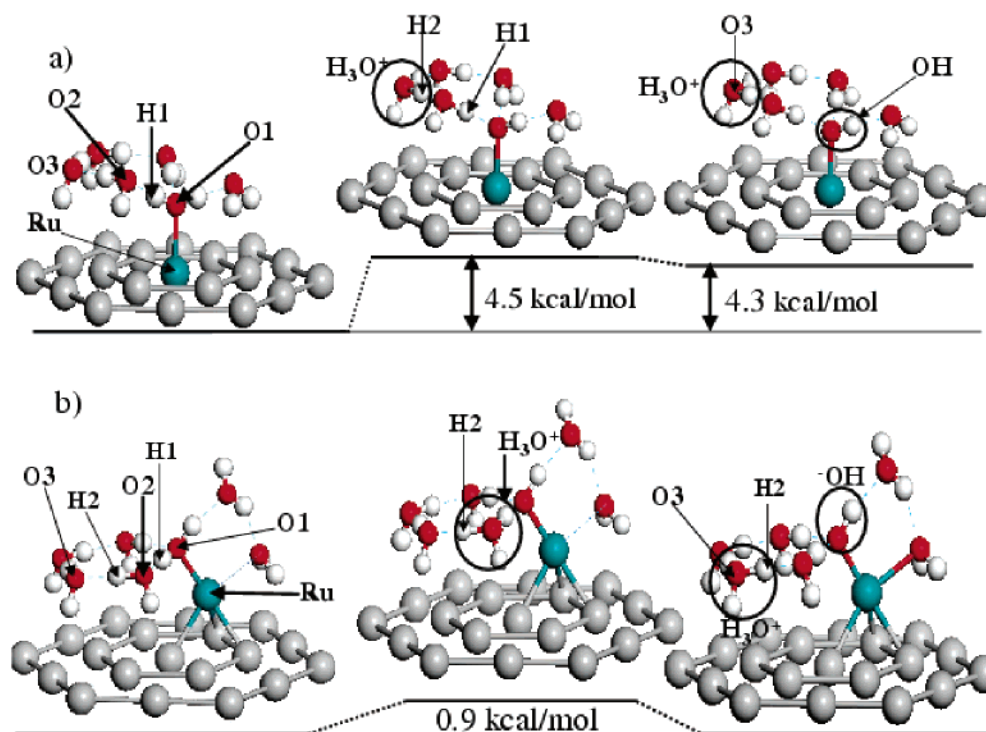
Figure 3. Geometrical arrangement of ambient water molecules around the $H_2O_{ads(Ru)}$ and calculated activation energies for the $H_2O_{ads(Ru)}$ dissociation on (a) alloy and (b) sequentially deposited Pt/Ru clusters.
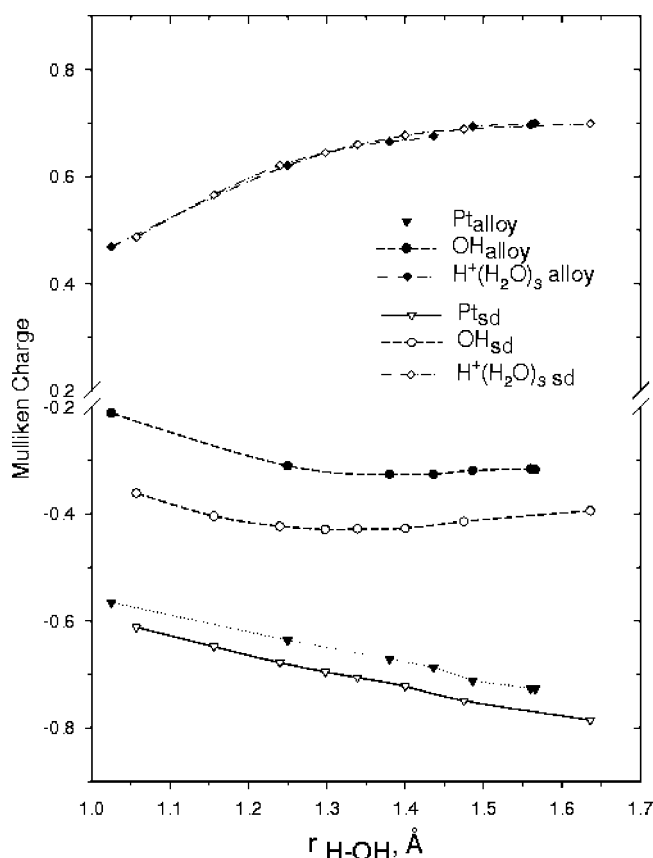

Figure 4. Plots of the Mulliken charges on $H^+(H_2O)_3$, $OH_{ads(Ru)}$, and Pt cluster, as a function of the dissociating O–H distance.

The heterolytic O–H bond cleavage of H_2O_{ads} over the different clusters is clearly favored by the stabilization of charged species by the ambient water and the effect of the secondary atom. The dissociation involves a synergic interaction between the Ru adatom and the H-bonded water shell. Although

still endothermic, the low activation barriers imply that the activation of water on bimetallic clusters should be readily accessible at room temperature. The sequentially deposited Pt/Ru nanocluster has the lowest barrier for the dissociation of H_2O_{ads}, in both gas and aqueous phases. Moreover, the remarkably low activation barrier, 0.9 kcal/mol, in aqueous media suggests that the sequentially deposited Pt/Ru nanocluster constitutes a more suitable material for the design of CO-tolerant anode catalysts.

4.3. CO_{ads} + OH_{ads} Reaction on Pure Pt(111) and Pt/Ru Bimetallic Clusters. 4.3.1. Solid–Gas Interface. The reaction energies and activation barriers were determined for the CO_{ads} + OH_{ads} → $COOH_{ads}$ reaction on pure Pt and bimetallic Pt/Ru clusters (Table 1). Parts a and b of Figure 5 display the energy profile and optimized structures of the reactant complex, TS, and product state for alloy and sequentially deposited Pt/Ru clusters, respectively. In the solid–gas interface, the intermediate $COOH_{ads}$ forms and remains adsorbed atop Pt atom but it should decompose readily to CO_{2ads} and H_{ads}. In a previous study,[46] the activation energies for the $COOH_{ads}$ → CO_{2ads} + H_{ads} were calculated on a pure Pt and on Pt/Ru alloy clusters. It was found that little energy (less than 0.1 eV) is required to break the COO–H bond on metal surfaces. In particular, for the sequentially deposited Pt/Ru nanocluster, the $COOH_{ads(Pt)}$ intermediate is bound to the Ru adatom through the oxygen atom of the hydroxyl group, facilitating the subsequent homolytic scission of the COO–H bond.

The most kinetically favorable pathway for the alloy involves the oxidation of $CO_{ads(Pt)}$ with OH_{ads} adsorbed on the Ru atom. The TS is located at the C1–O1 distances of 1.96 Å. The estimated activation energy and enthalpy for the $CO_{ads(Pt)}$ + $OH_{ads(Ru)}$ reaction on the alloy are, respectively, 6.4 and −1.9 kcal/mol. In contrast, the $CO_{ads(Pt)}$ oxidation on the sequentially deposited Pt/Ru cluster is predicted to be a considerably more difficult process, even though Hayden et al.[22] in their UHV experiments on ruthenium modified Pt(111) surfaces identified
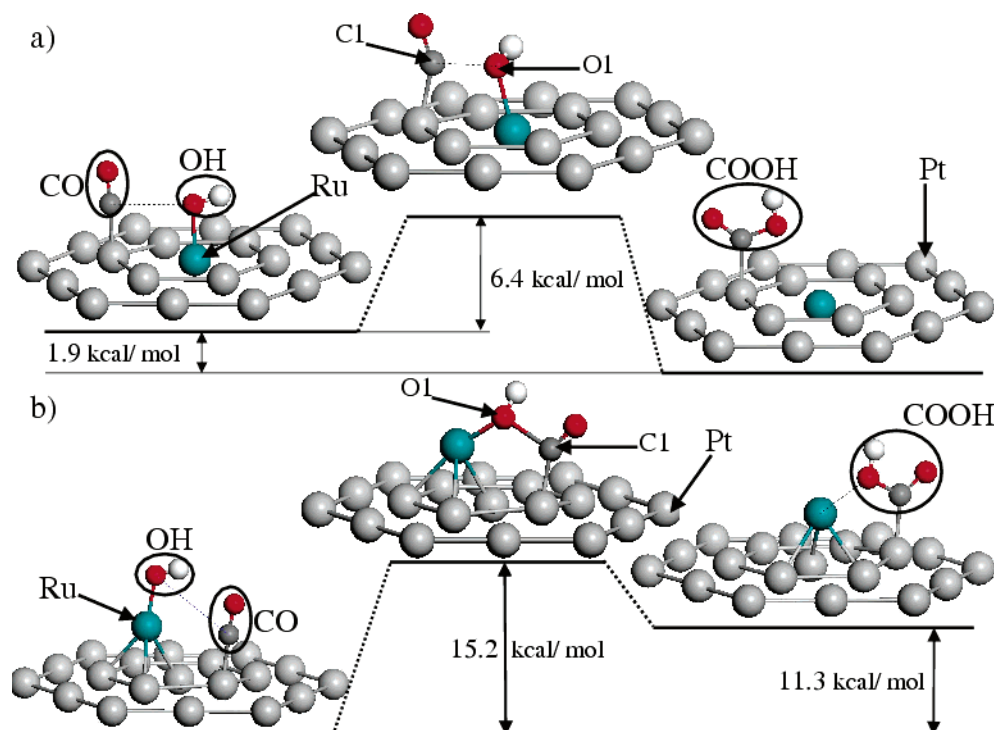
Figure 5. Schematic illustration of the calculated activation barriers and reaction energies for the $CO_{ads(Pt)} + OH_{ads(Ru)}$ reaction at the solid–gas interface on (a) alloy and (b) sequentially deposited Pt/Ru nanoclusters.

this route to be the kinetically favorable pathway. In the sequentially deposited Pt/Ru nanocluster, as in bulk Ru(0001), the strong OH adsorption ($E_{ads} \sim 70$ kcal/mol for OH_{ads} atop the Ru adatom) on the Ru adatom introduces a large barrier to $CO_{ads(Pt)}$ oxidation, 15.2 kcal/mol, with reaction endothermicity of 11.3 kcal/mol. The TS is found at the C1–O1 distances of 1.88 Å.

The $CO_{ads(Pt)} + OH_{ads(Pt)}$ reaction on Pt$_{38}$ is exothermic by 10.1 kcal/mol and proceeds readily despite the inability of pure Pt to dissociate water and produce oxidant OH_{ads} intermediate. The TS is located at the OC–OH distance of 1.95 Å. The barrier over the pure platinum cluster was found to be 5.3 kcal/mol, lower than in the bimetallic clusters, consistent with the fact that Pt(111) is a far superior catalyst for the oxidation of CO_{ads} to CO_2 in the presence of enough oxidant $OH_{ads(Pt)}$.

In Table 2, the activation barriers for the $CO_{ads} + OH_{ads}$ reaction on bulk Pt(111) from three independent DFT slab calculations are compared with those on the pure Pt$_{38}$ and alloy Pt$_{37}$Ru clusters. The calculated binding energies of $CO_{ads(Pt)}$ are nearly the same for the Pt$_{38}$ cluster and bulk Pt(111) surfaces, 37 kcal/mol (see section 4.1) and 38 kcal/mol,[27] respectively. However, the $CO_{ads(Pt)} + OH_{ads(Pt)}$ reaction on bulk Pt(111) is more difficult than on Pt$_{38}$ cluster since the $OH_{ads(Pt)}$ is much more strongly adsorbed on bulk Pt(111) and fails to promote the oxidative removal of $CO_{ads(Pt)}$. At solid–gas interface, the surface-mediated $CO_{ads} + OH_{ads}$ reaction on Pt$_{38}$ cluster has only half the activation energy reported by Koper et al.[27] for bulk Pt(111).

When the three independent slab calculations are compared, a curious disparity emerges. Over bulk Pt(111), the activation energies obtained by these independent calculations exhibit a significant departure of Desai and Neurock's results[47] from those of Hu et al.[49] and Koper et al.[27] Note that computational methods are nearly identical among the three studies. While the activation barriers computed by Hu et al. and Koper et al. for the $CO_{ads} + OH_{ads}$ reaction on bulk Pt(111) are in reasonable agreement (10–13 kcal/mol), Desai and Neurock's value (20.6 kcal/mol) differs

considerably from the other two. The activation energy for $H_2O_{ads(Pt)}$ dissociation reported by Desai and Neurock is again twice as large as that obtained by Michaelides and Hu.[48] The results strongly indicate that the activation barriers computed by Desai and Neurock are grossly overestimated. Given the large discrepancy over bulk Pt(111), it is reasonable to assume that the activation energies over Pt/Ru alloy reported by Desai and Neurock are equally overestimated.

On the basis of these results, it is concluded that pure Pt nanoclusters offer the most catalytically active surface for the $CO_{ads} + OH_{ads}$ combination, followed closely by the alloy. Clearly, in the solid–gas interface, the rate-determining step for pure Pt and alloy clusters is the formation of oxidant OH_{ads}, while the $CO_{ads} + OH_{ads}$ step proceeds rapidly once the OH_{ads} intermediate is generated on surface. In contrast, on the sequentially deposited Pt/Ru, the $CO_{ads(Pt)} + OH_{ads(Ru)}$ is the reaction that limits the rate of the overall process.
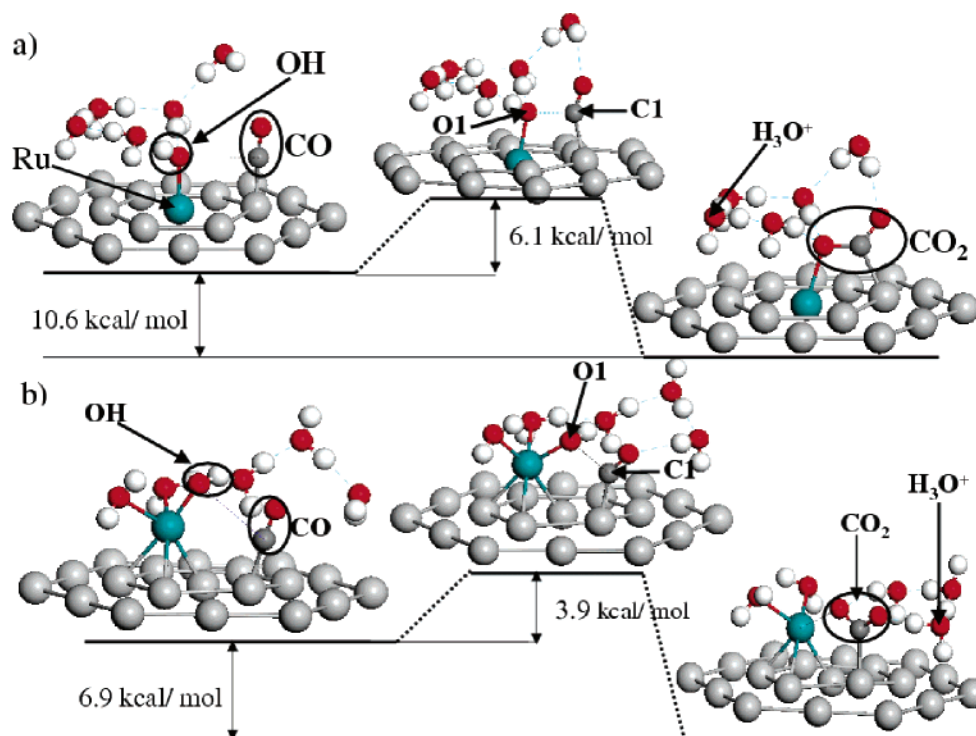
4.3.2. Microsolvated Environment. In the microsolvated environment, the $COOH_{ads(Pt)}$ intermediate dissociates spontaneously, leading to CO_2 adsorbed on the Pt site, a proton that migrates into the ambient water phase, and an electron delocalized in the entire metal cluster (eq 4):

$$CO_{ads(Pt)} + OH_{ads(M)} \rightarrow (COOH)_{ads(Pt)} \rightarrow$$
$$CO_{2ads(Pt)} + H^+_{(solv)} + e^-, \quad M = Ru/Pt \quad (4)$$
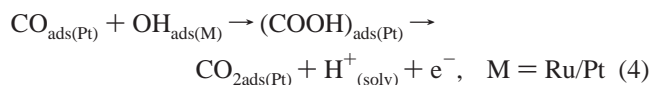
This is in agreement with the slab calculations by Hu and co-workers.[49] The authors found no barrier for the COOH disproportionation within a mixed phase $CO + 2OH + H_2O$. The formation of the stable compound CO_2 makes the reaction typically more exothermic than it is in the vapor phase, as observed in alloy, and especially in the sequentially deposited Pt/Ru nanocluster. The activation barriers and reaction energies for the CO_{ads} oxidation on the various clusters are listed in Table 1.

Parts a and b of Figure 6 show the optimized structures for the $CO_{ads(Pt)} + OH_{ads(Ru)}$ reaction in a microsolvated environment

Pure Pt and Bimetallic Pt/Ru Nanoclusters

J. Phys. Chem. B, Vol. 109, No. 49, 2005 **23577**

Figure 6. Energy profile of $CO_{ads(Pt)} + OH_{ads(Ru)}$ reaction in a microsolvated environment on (a) alloy and (b) sequentially deposited Pt/Ru nanoclusters.

for alloy and sequentially deposited Pt/Ru clusters, respectively. The favored adsorption sites for the $CO_{ads(Pt)}$ and $OH_{ads(Ru)}$ in this environment are the same as those in the vapor phase. The transition state is reached when the C1−O1 distances are 1.96 and 2.00 Å, respectively, for the alloy and sequentially deposited Pt/Ru clusters. In both cases, the nascent CO_2 remains atop the same Pt site that bound CO_{ads} but also interacts partially with the Ru atom via one of its oxygen atoms.

The energetics of H_2O_{ads} dissociation is significantly affected by the presence of ambient water molecules. In contrast, the activation barriers for the reaction $CO_{ads} + OH_{ads}$ in alloy and pure Pt are nearly unaffected by the change of environment. In the sequentially deposited Pt/Ru cluster, however, the presence of ambient water molecules markedly lowers the activation energy for the $CO_{ads(Pt)} + OH_{ads(Ru)}$ reaction. Interestingly, it is found that the degree of saturation (with water molecules) of the Ru coordination sites plays an important role in the energetics of the $CO_{ads(Pt)} + OH_{ads(Ru)}$ reaction. With saturation of the coordination sites of Ru adatom by two water molecules (see Figure 6b), the activation barrier drops dramatically, to nearly 3.9 kcal/mol, with the reaction exothermicity of 6.9 kcal/mol. However, if only one water molecule is coordinated to the Ru adatom, the activation barrier increases to over 9 kcal/mol. In an electrochemical environment, it is reasonable to assume that most of the Ru adatoms are in their fully hydrated state, facilitating therefore the oxidative removal of CO_{ads}. Obviously, this situation is not possible in alloy because the alloyed Ru atom has only one site for water coordination and the subsequent oxidant OH_{ads} formation.

In alloy, quantitative convergence in activation energies is achieved with five water molecules surrounding the reactants (Figure 6a). The estimated activation barrier for the $CO_{ads(Pt)} + OH_{ads(Ru)}$ reaction is 6.1 kcal/mol. The reaction is exothermic by 10.6 kcal/mol, five times larger than in solid−gas interface (1.9 kcal/mol), due to the formation of stable CO_{2ads}. Over the (111) surface of a bulk $Pt_{66.7\%}Ru_{33.3\%}$ alloy, Desai and Neurock[47] earlier reported the activation energy 14.3 kcal/mol and reaction

exothermicity of 1.4 kcal/mol for the $CO_{ads(Pt)} + OH_{ads(Ru)}$ reaction in aqueous media (Table 2), in sharp contrast to our results.

5. Conclusions

This study has demonstrated what makes a particular surface morphology especially tolerant toward CO poisoning. The energetics of the homolytic and heterolytic O−H bond cleavage of adsorbed water and the $CO_{ads} + OH_{ads}$ combination have been studied in pure Pt and on alloyed and sequentially deposited Pt(111)/Ru nanoclusters. Calculations were performed in vapor phase and in a microsolvated environment to elucidate which surface morphology is more CO-tolerant. Some insights have been gained through all these calculations. The results provide strong evidence of higher catalytic activity in the sequentially deposited Pt/Ru than in the alloy Pt/Ru. The origin of the apparent high catalytic activity of sequentially deposited Pt/Ru is ascribed to the presence of an under-coordinated Ru adatom on the Pt principal cluster.

The study provides, at the atomic level, a qualitative understanding of the elementary steps in the removal of CO_{ads} that occur in bimetallic Pt/Ru nanoclusters of varying surface morphology. The importance of aqueous environment in facilitating the removal of CO_{ads} under the *bifunctional mechanism* is explained. In particular, for the sequentially deposited Ru on Pt nanocluster, the degree of hydration of the Ru adatom plays an important role in the energetics of the $CO_{ads(Pt)} + OH_{ads(Ru)}$ reaction, allowing the first step, the activation of water, to be nearly a barrierless process.

References and Notes

(1) Lemons, R. A. *J. Power Sources* **1990**, *29*, 251.

(2) Watanabe, M.; Motoo, S. *J. Electroanal. Chem.* **1975**, *60*, 267.

(3) Watanabe, M.; Motoo, S. *J. Electroanal. Chem.* **1975**, *60*, 275.

(4) Zhu, Y.; Uchida, H.; Watanabe, M. *Langmuir* **1999**, *15*, 8757.

(5) Watanabe, M.; Zhu, Y.; Uchida, H. *J. Phys. Chem. B* **2000**, *104*, 1762.

(6) Gasteieger, H. A.; Markovic, N. M.; Ross, P. N.; Cairns, E. J., Jr. *J. Phys. Chem.* **1994**, *98*, 617.

(7) Rolison, D. R. *Langmuir* **1999**, *15*, 774.

(8) Kabbabi, A.; Faure, R.; Durand, R.; Beden, B.; Hahn, F.; Leger, J. M.; Lamy, C. *J. Electroanal. Chem.* **1998**, *444*, 41.

(9) Buatier de Mongeot, F.; Scherer, M.; Gleich, B.; Kopatzki, E.; Behm, R. J. *Surf. Sci.* **1998**, *411*, 249.

(10) Chrzanowski, W.; Wieckowski, A. *Langmuir* **1998**, *14*, 1967.

(11) Lin, W. F.; Zei, M. S.; Eiswirth, M.; Ertl, G.; Iwasita, T.; Vielstich, W. *J. Phys. Chem. B* **1999**, *103*, 6968.

(12) Davies, J. C.; Hayden, B. E.; Pegg, D. *J. Electrochim. Acta* **1998**, *44*, 1181.

(13) Rodriguez-Nieto, F. J.; Morante-Catacora, T. Y.; Cabrera, C. R. *J. Electroanal. Chem.* **2004**, *571*, 15.

(14) Hohenberg, P.; Kohn, W. *Phys. Rev.* **1964**, *136*, B864.

(15) Kohn, W.; Sham, L. J. *Phys. Rev.* **1965**, *140*, A1133.

(16) Delley, B. *J. Chem. Phys.* **1990**, *92*, 508.

(17) Delley, B. *J. Chem. Phys.* **2000**, *113*, 7756.

(18) Perdew, J. P.; Burke, K.; Ernzerhof, M. *Phys. Rev. Lett.* **1996**, *77*, 3865.

(19) Delley, B. *Int. J. Quantum Chem.* **1998**, *69*, 423.

(20) Dunlap, B. I.; Rösch, N. *Adv. Quantum Chem.* **1990**, *21*, 317.

(21) Sellers, H.; Pattrito, E. M.; Paredes-Olivera, P. *Surf. Sci.* **1998**, *418*, 376.

(22) Davies, J. C.; Hayden, B. E.; Pegg, D. J.; Rendall, M. E. *Surf. Sci.* **2002**, *496*, 110.

(23) Lin, W. F.; Zei, M. S.; Eiswirth, M.; Ertl, G.; Iwasita, T.; Vielstich, W. *J. Phys. Chem. B* **1999**, *103*, 6968.

(24) Orita, H.; Itoh, N.; Inada, Y. *Chem. Phys. Lett.* **2004**, *384*, 271.

(25) Kresse, G.; Gil, A.; Sautet, P. *Phys. Rev. B* **2003**, *68*, 073401.

(26) Feibelman, P. J.; Hammer, B.; Nørskov, J. K.; Wagner, F.; Scheffler, M.; Stumpf, R.; Watwe, R.; Dumesic, J. *J. Phys. Chem. B* **2001**, *105*, 4018.

(27) Shubina, T. E.; Hartnig, C.; Koper, M. T. M. *Phys. Chem. Chem. Phys.* **2004**, *6* (16), 4215.

(28) Janssen, M. M. P.; Moolhuysen, J. *J. Catal.* **1977**, *46*, 289.

(29) Ishikawa, Y.; Diaz-Morales, R. R.; Perez, A.; Vilkas, M. J.; Cabrera, C. R. *Chem. Phys. Lett.* **2005**, *411*, 404.

(30) Sexton, B. A.; Hughes, A. E. *Surf. Sci.* **1984**, *140*, 227.

(31) Michaelides, A.; Ranea, V. A.; de Andres, P. L.; King, D. A. *Phys. Rev. Lett.* **2003**, *90*, 216102.

(32) Ishikawa, Y.; Liao, M.-S.; Cabrera, C. R. *Surf. Sci.* **2002**, *513*, 98.

(33) Shustorovich, E.; Sellers, H. *Surf. Sci. Rep.* **1998**, *31*, 1.

(34) Meng, S.; Xu, L. F.; Wang, E. G.; Gao, S. *Phys. Rev. Lett.* **2002**, *89*, 176104.

(35) Ogasawara, H.; Brena, B.; Nordlund, D.; Nyberg, M.; Pelmenschikov, A.; Petterson, L.; Nilsson, A. *Phys. Rev. Lett.* **2002**, *89*, 276102.

(36) Bedürftig, K.; Völkening, S.; Wang, Y.; Wintterlin, J.; Jacobi, K.; Ertl, G. *J. Chem. Phys.* **1999**, *111*, 11147.

(37) Gdowski, G. E.; Fair, J. A.; Madix, R. J. *Surf. Sci.* **1983**, *127*, 541.

(38) Feibelman, P. J. *Science* **2002**, *295*, 99.

(39) Michaelides, A.; Alavi, A.; King, D. A. *J. Am. Chem. Soc.* **2003**, *125*, 2746.

(40) Weissenrieder, J.; Mikkelsen, A.; Andersen, J. N.; Feibelman, P. J.; Held, G. *Phys. Rev. Lett.* **2004**, *93*, 196102.

(41) (a) Anderson, A. B.; Neshev, N. M.; Sidik, R. A.; Shiller, P. *Electrochim. Acta* **2002**, *47*, 2999. (b) Anderson, A. B.; Grantscharova, E. *J. Phys. Chem.* **1995**, *99*, 9143. (c) Anderson, A. B.; Grantscharova, E. *J. Phys. Chem.* **1995**, *99*, 9149.

(42) Wang, Y.; Balbuena, P. B. *J. Phys. Chem. B* **2004**, *108*, 4376.

(43) Zundel, G. *The Hydrogen Bond— Recent Developments in Theory and Experiments II*; Schuster, P., Zundel, G., Sandorfy, C., Eds.; North-Holland: Amsterdam, 1976; pp 683−766.

(44) Eigen, M.; Kruse, W.; De Maeyer, L. *Prog. React. Kinet.* **1964**, *2*, 285.

(45) Marx, D.; Tuckerman, M.; Hutter, J.; Parrinello, M. *Nature* **1999**, *397*, 601.

(46) Ishikawa, Y.; Liao, M.-S.; Cabrera, C. R. *Surf. Sci.* **2000**, *463*, 66.

(47) Desai, S.; Neurock, M. *Electrochim. Acta* **2003**, *48*, 3759.

(48) Michaelides, A.; Hu, P. *J. Am. Chem. Soc.* **2001**, *123*, 4235−4242.

(49) Gong, X.-Q.; Hu, P.; Raval, R. *J. Chem. Phys.* **2003**, *119*, 6324.